Highlights

All-fiber hollow-core fiber gas cell

Dmytro Suslov,Matěj Komanec,Thomas William Kelly,Ailing Zhong,Stanislav Zvánovec,Francesco Poletti,Natalie Wheeler,Radan Slavík

- All-fiber hollow-core fiber gas cell is developed
- The gas cell is compact, easily transportable, and long-term stable
- Low-loss single-mode to hollow-core fiber interconnection with a gas inlet is prepared
- Gas samples can be easily filled into the hollow-core fiber-based gas cell

All-fiber hollow-core fiber gas cell

Dmytro Suslov[a], Matěj Komanec[a], Thomas William Kelly[b], Ailing Zhong[a], Stanislav Zvánovec[a], Francesco Poletti[b], Natalie Wheeler[b] and Radan Slavík[b,*]

[a]Czech Technical University in Prague, Faculty of Electrical Engineering, Department of Electromagnetic Field, Technicka 2, Prague, 16627, Czech Republic

[b]Optoelectronics Research Centre, University of Southampton, Southampton, SO17 1BJ, The United Kingdom

ARTICLE INFO

Keywords:
gas cell
hollow core fiber
higher-order modes
low loss coupling

ABSTRACT

We present a hollow-core fiber (HCF) gas cell with light launched and collected via standard solid-glass core single-mode fibers (SMFs). Gas delivery is realized via a 100 μm gap between the SMF and HCF with light low-loss coupling optimized for such a gap. Coupling into higher-order modes as well as the Fresnel reflections at the SMF-HCF interface are strongly suppressed to minimize unwanted multi-path interference. The assembled HCF gas cell including the gas inlet is encapsulated in a conventional metallic T-piece for easy gas filling, venting, and sealing. Thanks to its numerous features, such as alignment-free design (once fabricated), above-described promising optical performance, and compactness, we believe it will be of interest for applications in gas sensing and as gas references.

1. Introduction

Gas sensing using hollow-core fibers (HCFs) has been shown (1) to enable gas detection at sub-ppb sensitivities (2) thanks to the long-length gas-light interaction. In the research laboratories, light is usually coupled to and from the HCF using free-space coupling via an optical window/lens embedded in the gas cell (3; 4; 5). However, practical gas cells would ideally be alignment-free (once fabricated). Thus in most applications, light delivery to and from the gas cell is expected to be via standard optical fibers optimized for the wavelength range of interest (6; 5; 7). However, there are several challenges to achieving this.

The first challenge is associated with the gas filling time, which is significantly reduced when using HCFs with large core diameters, such as the state-of-the-art antiresonant fibers (8). A large core implies a large mode-field diameter (MFD) of the HCF fundamental guided mode. Thus, the interconnection between the delivery fiber and the HCF needs to accommodate for the difference in the MFDs of these two fibers. Besides low insertion loss, it is also important to minimize coupling into higher-order modes to avoid multi-path interference that degrades the performance, especially in absorption spectroscopy (6).

A further challenge lies in delivering the gas sample to the HCF. For an HCF gas cell spliced to delivery (solid-core) fibers, this can be done, e.g., via the drilling of side holes (5) or by splitting the HCF into shorter segments (6). Another solution represents the 'mechanical connection' of the HCF and delivery fibers, leaving a small gap between them (5; 9; 10). However, such a configuration requires further effort to ensure long-term stability. This can be addressed via gluing (11). In all these reports, MFD matching that takes into account the gap between the delivery fiber and the HCF was not considered, allowing for only very small (1-3 μm) gaps.

The last key challenge is the Fresnel back reflection. For example, for silica single-mode fibers (SMFs), light travels from silica (refractive index $n = 1.45$ at 1550 nm) to air in HCF ($n = 1$), causing a 3.5 % Fresnel back reflection. When such reflections are at both the input and output of the gas cell, it causes parasitic Fabry-Perot resonances, leading to significant degradation in the gas cell performance. These back reflections can be suppressed when delivery fibers are anti-reflection (AR) coated (1) or angle-cleaved (12). Angle-cleaving in the context of gas cells was reported to increase the insertion loss and higher-order mode coupling. This could be addressed by angle-aligning the HCF with angle-cleaved delivery fiber or combining it with angle-cleaving with AR coatings, which was demonstrated to provide the necessary gap for gas delivery (13). However, such connections have not yet been demonstrated to enable gas delivery in the form of a gas cell.

As elaborated above, there are reports on addressing one or two of the above three challenges or having the potential to address all three. However, to the best of our knowledge, none of the solutions has been demonstrated to address all of the challenges at the same time while ensuring robustness and performance stability.

Here, we propose an all-fiber HCF gas cell that addresses all three key challenges mentioned above. It is based on the HCF interconnection technique we showed to have 0.15 dB SMF-HCF loss that was reciprocal for HCF-SMF, with back-reflection levels well below -30 dB and suppressed parasitic coupling into higher-order modes (14). Its schematics is presented in Fig. 1a, showing a short segment (1/4 pitch) of a graded index multi-mode fiber (GRIN) serving as a mode field adapter between the SMF and HCF. The GRIN is spliced with the SMF and an AR coating is deposited on its surface. This assembly is then aligned using 5D stages (x,y,z, pitch, and yaw) with the HCF, and the entire assembly is glued together.

*Corresponding author
ORCID(s): 0000-0002-9336-4262 (R. Slavík)

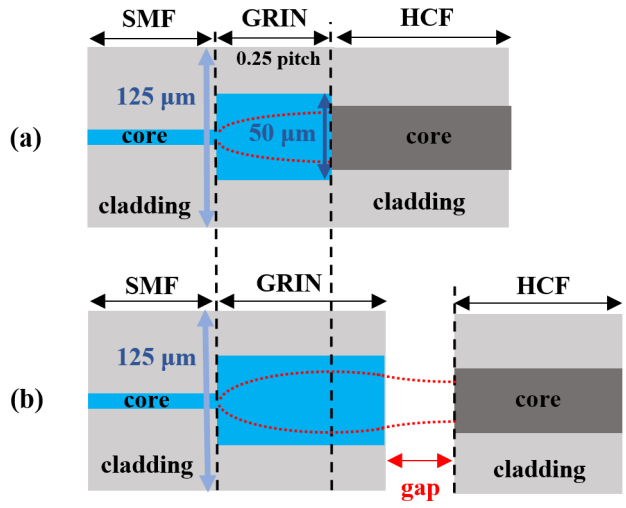

Figure 1: Schematics of the SMF-HCF connection that (a) includes mode-field adaptation using 1/4-pitch long GRIN with AR-coating, directly glued on the HCF (14) and (b) GRIN longer than 1/4 pitch with AR-coating that produces optimum coupling into the HCF via a small gap (15), suitable for gas filling.

During gluing, the insertion loss was reported to be negligible (within 0.01 dB (14)) and showed long-term stability over several months and also during thermal cycling (16).

We recently demonstrated how this low insertion loss technique could be modified to obtain an air gap between SMF and HCF while maintaining low-loss interconnection (15). It is schematically shown in Fig. 1b. By using GRIN which is slightly longer than 1/4 pitch, the output beam is slightly focusing, reaching the beam waist at a certain distance, where the light is low-loss coupled into the HCF. This distance creates an air gap, which we suggest here to use for gas delivery into the HCF. We show how the gas delivery is enabled while keeping the excellent stability of the interconnection. The interconnection with the gas inlet is subsequently inserted into a standard metallic T-piece to enable easy and controllable gas delivery (17). In a proof-of-principle demonstration, we show a 10-m-long gas cell with parasitic Fabry-Perot resonances strongly suppressed and an air gap of 100 μm for gas delivery. We believe that the developed platform will be of interest to gas cells such as for frequency references and ultra-sensitive gas sensing.

2. Gas cell design and assembly

We first connect SMF pigtails to both HCF ends. A detail of the SMF-HCF connection is shown in Fig. 2. For the adaptation of the MFD between the SMF and HCF, we splice a short piece of a GRIN multimode fiber onto the SMF first (15), Fig. 2. As discussed earlier, we use GRIN slightly longer than 1/4 pitch to achieve low-loss coupling while having a small gap between the HCF and the GRIN (15). This gap enables gas ingress/egress from the HCF.

In practice, the process of our SMF-HCF connection, Fig. 2, consists of gluing SMF+GRIN and HCFs into two 1.00-mm outer diameter glass capillaries (blue in Fig. 2) that are subsequently inserted into an overlap glass capillary (grey in Fig. 2). This outer glass capillary has a hole filed on its side for gas delivery (Fig. 2). The inner diameter of the overlap capillary is 1.05 mm, which is 50 µm larger than the outer diameter of the inserted 1.00 mm capillaries. This gives enough room for aligning the SMF+GRIN with the HCF but is small enough to enable subsequent gluing without losing the alignment (13).

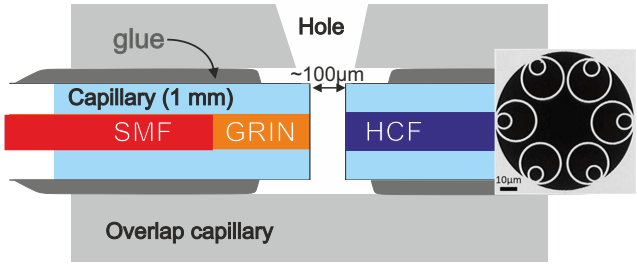

Figure 2: Gas cell interconnection assembly: Overlap capillary (grey) with two capillaries containing HCF and SMF+GRIN (blue) aligned and glued inside it.

As for the GRIN fiber, we used OM2 multimode fiber, which we spliced to SMF-28 and glued into the 1 mm diameter, 5 mm long capillary. Subsequently, we polished it to the desired GRIN fiber length of ~310 µm (30 µm longer than quarter pitch to obtain desired GRIN-HCF gap of 100 µm (15)). We created four samples, where two were then deposited with an AR coating (4-layers SiO_2/TiO_2 with a minimum reflection at 1550 nm). The AR coating not only allows suppression of Fresnel losses which contribute to 0.16 dB insertion loss on each HCF-SMF connection, but primarily reduces the parasitic Fabry-Perot etalon effect.

The measured back-reflection from AR-coated SMF-GRINs is shown in Fig. 3 together with the back-reflection expected from the uncoated samples. We see the minimum reflection at 1568 nm with a back-reflection level at -38 dB. This is a good value for AR coatings, but can be further lowered below -60 dB (considered as reflection-free level) by having an angled interface or by combining the angled interface with AR coating, as we demonstrated in (13).

We used a 10 m long, 6-tube nested anti-resonant nodeless fiber (NANF) with the core size of 34 µm (corresponding MFD of ~24 µm at 1550 nm) and the measured attenuation of ~0.35 dB/km at 1550 nm. The HCF structure is visible in Fig. 2. For the HCF, it was first cleaved and then glued into a similar glass capillary as the SMF+GRIN (1 mm outer diameter and 5 mm length).

Figure 4 shows the glued SMF+GRIN-HCF assembly prior to encapsulation into the metallic T-piece to enable controlled gas delivery. For this, we used a small 3-port metallic T-piece from Swagelok Ltd., Fig. 5. The metallic T-piece contained two neoprene rubber seal feed-throughs for fibers (Spectite Ltd.) and the third port allowed connection

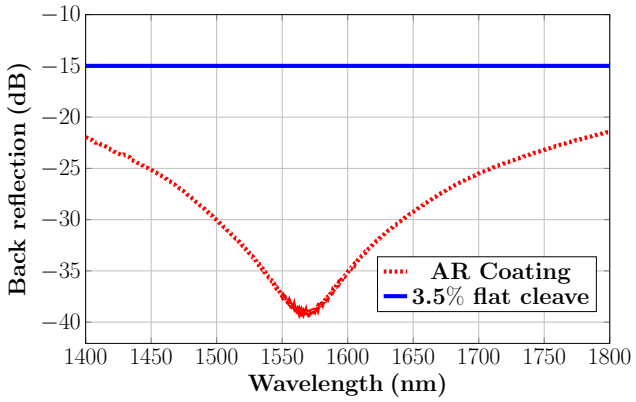

Figure 3: Measured back-reflection of the AR-coated SMF+GRIN mode-field adapter compared to a flat surface of an uncoated mode-field adapter.

to the gas delivery system. The entire component is rated to withstand 200 bar of pressure. We have created two HCF gas cells - one with and one without AR coating.

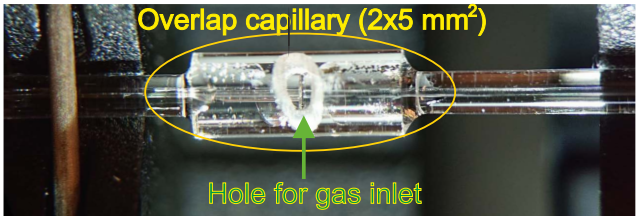

Figure 4: Photo of the aligned and glued gas cell SMF+GRIN-HCF coupling.

3. Gas cell characterization

Following the assembly, we measured the gas cell transmission over a broad wavelength range of 1300-1700 nm using a supercontinuum source (SC, Fianium SC400), see the measurement setup in Fig. 6. Particularly prominent spectral features were observed in the 1300–1400 nm band, which showed absorption dips due to water vapor presence in the HCF. We show detail over the 5 nm spectral window in Fig. 7, where we purged the gas cell with Argon for 2 hours and subsequently up to 19 hours, observing the expected reduction of the water absorption dips, without any observable indication of the gas cell performance degradation in terms of optical losses.

Demonstration of the absence of the parasitic Fabry-Perot resonances requires spectral analysis with better resolution than offered by our OSA (0.01 nm corresponding to 1.25 GHz at 1550 nm), as they are expected to have a period of 15 MHz for our HCF length of 10 m (considering refractive index of an air-filled HCF core). For this purpose, we use a continuously sweeping laser (EXFO T100S-HP) as a source and a photodiode at the detection side connected to an oscilloscope. For wavelength, we chose 1480–1481 nm, which was a compromise between the wavelength range at

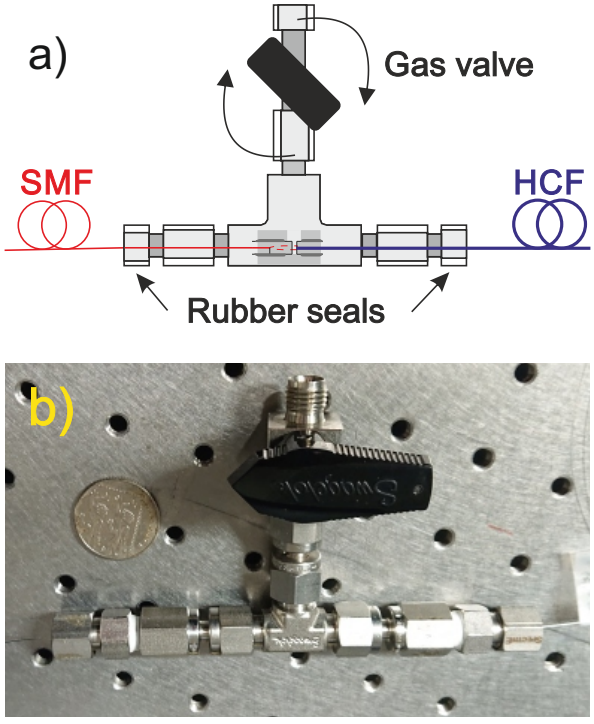

Figure 5: a) Schematic and b) photo of the finished SMF+GRIN-HCF assembly in the T-piece that allows for gas delivery.

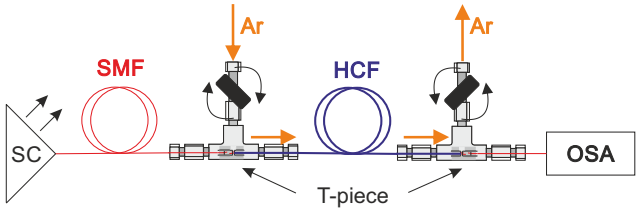

Figure 6: Water peak absorption measurement setup for absorption spectroscopy using prepared HCF gas cells.

which our AR coating operated (1500–1650 nm for back-reflection <-30 dB, with 1480 nm showing only slightly-worse value of -28 dB, Fig. 2) and region with prominent water absorption dips (1300–1480 nm). Results obtained with both prepared gas cells (with and without AR coatings) showing two water absorption dips are shown in Fig. 8.

We can observe that the parasitic Fabry-Perot resonances in the gas cell without AR coating cause fast changes in the transmission of as much as 7.5%. These parasitic resonances are not observed in the gas cell with AR-coating, in which the power fluctuations seem to be limited by random noise, most probably due to the stability of the sweeping laser. Further, we do not see any power fluctuations due to multi-path interference due to higher-order modes, which is expected to have a period of 0.2 nm (for LP_{11}-LP_{01} interference with LP_{11} mode attenuation of 35 dB/km) and 0.1 nm (LP_{02}-LP_{01}-interference with LP_{02} attenuation of 2100 dB/km).

We have not studied gas cell performance under low-pressure or vacuum conditions, where outgassing of the used

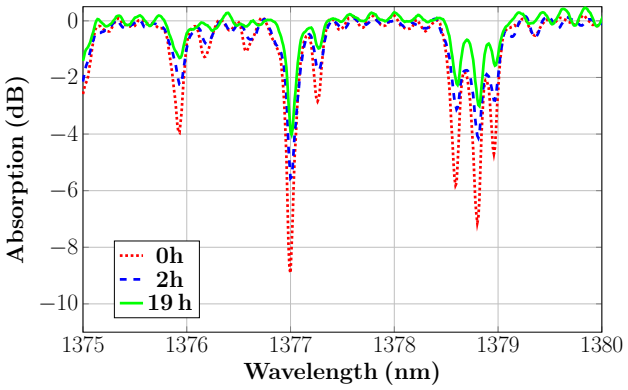

Figure 7: Measured transmission spectra of the HCF gas cell during purging with Argon.

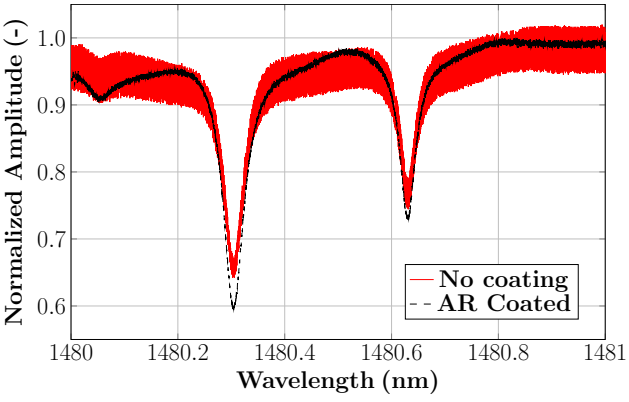

Figure 8: Gas cell transmission measured at high resolution for gas cells with AR-coatings and without coating, showing parasitic Fabry-Perot resonances.

glue may pose limitations to the achievable level of the vacuum. This will be the subject of our follow-up study.

4. Conclusion

We have developed compact all-fiber HCF gas cells, which require no alignment after the initial assembly. The gas cells are based on active alignment and subsequent gluing, which minimizes coupling into higher-order modes (thus minimizing multi-path interference). Furthermore, we applied anti-reflective coatings, which led to significant suppression of parasitic Fabry-Perot resonances. As these two effects were previously identified as two major limitations to all-fiber HCF gas cells (6), the presented approach promises to achieve high sensitivities (e.g., ppb-level of gas detection), previously possible only with free-space-optics interrogated HCF gas cells.

CRediT authorship contribution statement

Dmytro Suslov: Gas cell preparation, Experimental work, Writing - original draft. **Matěj Komanec:** Mode-field adapter design, Writing - original draft. **Thomas William Kelly:** Experiment, Writing - review. **Ailing Zhong:** GRIN mode-field adapter preparation, Writing - review. **Stanislav Zvánovec:** Writing - review. **Francesco Poletti:** Hollow-core fiber design, Writing - review. **Natalie Wheeler:** Experiment design, Gas filling, Writing - review. **Radan Slavík:** Data analysis, Experimental concept, Writing - original draft and review.

5. Declaration of Competing Interest

The authors declare that they have no known competing financial interests or personal relationships that could have appeared to influence the work reported in this paper.

6. Data availability

Data are available on request.

7. Acknowledgements

This work was funded by the GACR project 22-32180S, International Mobility of Researchers in CTU project number CZ.02.2.69/0.0/0.0/18_053/0016980 and by the EPSRC projects EP/P030181/1, EP/W037440/1, and EP/X011674/1.

References

[1] W. Jin, H. Bao, P. Zhao, Y. Zhao, Y. Qi, C. Wang, H. Ho, Recent advances in spectroscopic gas sensing with micro/nano-structured optical fibers, Photonic Sensors 11 (2021) 1–17.

[2] P. Zhao, Y. Zhao, H. Bao, H. Ho, W. Jin, S. Fan, S. Gao, Y. Wang, P. Wang, Mode-phase-difference photothermal spectroscopy for gas detection with an anti-resonant hollow-core optical fiber, Nature Communications 11 (02 2020).

[3] P. Jaworski, P. Koziol, K. Krzempek, D. Wu, F. Yu, P. Bojęś, G. Dudzik, M. Liao, K. Abramski, J. Knight, Antiresonant hollow-core fiber-based dual gas sensor for detection of methane and carbon dioxide in the near-and mid-infrared regions, Sensors 20 (2020) 3813.

[4] W. Thomas, P. Horak, I. Davidson, M. Partridge, G. Jasion, S. Rikimi, A. Taranta, D. Richardson, F. Poletti, N. Wheeler, Controlling the attenuation of hollow core fibers using gas-induced differential refractive index, 2021.

[5] M. Nikodem, Laser-based trace gas detection inside hollow-core fibers: A review, Materials (Basel, Switzerland) 13 (09 2020).

[6] J. Parry, B. Griffiths, N. Gayraud, E. McNaghten, A. Parkes, W. Macpherson, D. Hand, Towards practical gas sensing with micro-structured fibres, Measurement Science and Technology 20 (2009) 075301.

[7] P. Zhao, H. Ho, W. Jin, S. Fan, S. Gao, Y. Wang, P. Wang, Gas sensing with mode-phase-difference photothermal spectroscopy assisted by a long period grating in a dual-mode negative-curvature hollow-core optical fiber, Optics Letters 45 (2020) 5660–5663.

[8] G. T. Jasion, H. Sakr, J. R. Hayes, S. R. Sandoghchi, L. Hooper, E. N. Fokoua, A. Saljoghei, H. C. Mulvad, M. Alonso, A. Taranta, T. D. Bradley, I. A. Davidson, Y. Chen, D. J. Richardson, F. Poletti, 0.174 dB/km Hollow Core Double Nested Antiresonant Nodeless Fiber (DNANF), in: 2022 Optical Fiber Communications Conference and Exhibition (OFC), 2022, pp. 1–3.

[9] Z. Zhang, A. Jia, Y. Hong, W. Ding, S. Gao, Y. Wang, Ultralow-loss, plug-and-play hollow-core fiber interconnection, in: Optical Fiber Communication Conference (OFC) 2022, Optica Publishing Group, 2022, p. W4E.4.

[10] Q. Wang, Z. Wang, H. Zhang, S. Jiang, Y. Wang, W. Jin, W. Ren, Dual-comb photothermal spectroscopy, Nature Communications 13 (2022) 2181.

[11] F. Liu, H. Bao, H. L. Ho, W. Jin, S. Gao, Y. Wang, Multicomponent trace gas detection with hollow-core fiber photothermal interferometry and time-division multiplexing, Opt. Express 29 (26) (2021) 43445–43453.

[12] G. Miller, G. Cranch, Reduction of intensity noise in hollow core optical fiber using angle-cleaved splices, IEEE Photonics Technology Letters 28 (2015) 1–1.

[13] D. Suslov, E. N. Fokoua, D. Dousek, A. Zhong, S. Zvánovec, T. D. Bradley, F. Poletti, D. J. Richardson, M. Komanec, R. Slavík, Low loss and broadband low back-reflection interconnection between a hollow-core and standard single-mode fiber, Opt. Express 30 (20) (2022) 37006–37014.

[14] D. Suslov, M. Komanec, E. R. Numkam Fokoua, D. Dousek, A. Zhong, S. Zvánovec, T. D. Bradley, F. Poletti, D. J. Richardson, R. Slavík, Low loss and high performance interconnection between standard single-mode fiber and antiresonant hollow-core fiber, Scientific Reports 11 (8799) (2021).

[15] A. Zhong, M. Ding, D. Dousek, D. Suslov, S. Zvánovec, F. Poletti, D. J. Richardson, R. Slavík, M. Komanec, Gap design to enable functionalities into nested antiresonant nodeless fiber based systems, Opt. Express 31 (9) (2023) 15035–15044.

[16] D. Dousek, M. Komanec, A. Zhong, D. Suslov, S. Zvánovec, P. Veselý, Y. Chen, T. D. Bradley, E. R. N. Fokoua, F. Poletti, D. J. Richardson, R. Slavík, Long-term stability of hollow core to standard optical fiber interconnection, in: K. Kalli, A. Mendez, P. Peterka (Eds.), Micro-structured and Specialty Optical Fibres VII, Vol. 11773, International Society for Optics and Photonics, SPIE, 2021, p. 117731B.

[17] D. Suslov, T. W. Kelly, S. Rikimi, A. Zhong, A. Taranta, S. Zvánovec, F. Poletti, D. J. Richardson, M. Komanec, N. Wheeler, R. Slavík, Towards compact hollow-core fiber gas cells, in: Conference on Lasers and Electro-Optics, Optica Publishing Group, 2022, p. SW4K.2.